Geophysical Journal International

Geophys. J. Int. (2014) **198,** 1701–1713 doi: 10.1093/gji/ggu195
GJI Seismology

Fingerprinting ordered diffractions in multiply diffracted waves

Giovanni Angelo Meles and Andrew Curtis

School of Geosciences, University of Edinburgh, West Mains Road, Edinburgh EH9 3JW, United Kingdom. E-mail: gmeles@staffmail.ed.ac.uk

Accepted 2014 May 22. Received 2014 January 24; in original form 2013 July 4

SUMMARY

We show how to 'fingerprint' individual diffractors inside an acoustic medium using interrogative wave energy from arrays of sources and receivers. For any recorded multiply diffracted wave observed between any source and any receiver, the set of such fingerprints is sufficient information to identify all diffractors involved in the corresponding diffraction path, and the sequential order in which diffractors are encountered. The method herein thus decomposes complex, multiply diffracted wavefields into constituent, single-diffraction interactions.

Key words: Interferometry; Wave scattering and diffraction; Wave propagation; Acoustic properties.

1 INTRODUCTION

Scattering is the physical phenomenon where propagating energy, such as electromagnetic radiation, acoustic pressure or particle flux, is affected by the presence of perturbations in the properties of the medium through which they travel. Such perturbations are called scatterers, and depending on their spatial distribution they may cause different forms of energy redistribution such as reflection, refraction or diffraction of wavefield energy. Scattering theory is widely used to describe such phenomena in classical physics applications relying on Newton and Maxwell's equations, including radar sensing (Ferretti *et al.* 2001), medical ultrasound (Insana & Brown 1993) and geophysics (Yilmaz 2001), and is also important in the quantum physics of quantum mechanics (Chadan & Sabatier 1979).

Diffraction is the specific kind of scattering that occurs when an incident wavefield interacts with structures of small spatial extent relative to the wavelength. Within geophysics, diffraction may be caused by seismic waves interacting with subsurface angular boundaries between rocks of different elastic parameters or density, or with diffractors formed by voids (e.g. caves), faults or fractures (Landa *et al.* 1987; Kanasewich & Phadke 1988; Liu *et al.* 1997; Landa & Keydar 1998; Bansal & Imhof 2005).

The potential advantages of using diffracted waves for remote interrogation have been studied in diverse fields since the seminal works of Krey (1952) and Hagedoorn (1954). For example, within seismic migration, diffracted events are used to extract velocity information based on focusing properties of incorrectly migrated events (Harlan *et al.* 1984; de Vries & Berkhout 1984), or to perform migration velocity analysis by collapsing diffraction signatures (Sava *et al.* 2005). More recently, recognition of over- or undermigrated diffracted events was used in depth domain migration to provide updates to velocity models and diffractor locations (Coimbra *et al.* 2013). Moreover, diffractions are of particular interest as their processing can lead to superresolution and the recovery of details smaller than the seismic wavelength (Derode *et al.* 1995, 2001; Blomgren *et al.* 2002; Khaidukov *et al.* 2004). Similar approaches were also used to perform high-resolution imaging of the Earth's subsurface using electromagnetic ground penetrating radar data (Papziner & Nick 1998), and to identify geological strata which have particularly strong internal heterogeneity such as karstic carbonates (Grasmueck *et al.* 2012). It is therefore often important to identify diffracted events in recorded data, and algorithms have been designed to discriminate diffracted from reflected wave energy (Landa *et al.* 1987; Fomel *et al.* 2006; Fomel 2007; de Figueiredo *et al.* 2013).

While in theory all scattered waves provide useful information, in practice any distribution of strong diffractors also results in inter-diffractor wavefield interactions in a process known as multiple-diffraction. Recorded wavefields are then potentially extremely complex, even for a low number of diffractors. Several studies have developed methods to interpret (Harlan *et al.* 1984; Landa & Keydar 1998; Soellner & Yang 2002; Khaidukov *et al.* 2004; Shtivelman & Keydar 2004; Sava *et al.* 2005; Taner *et al.* 2006; Fomel 2007; Moser & Howard 2008; Dell & Gajewski 2011) or simply ignore (Klem-Musatov 1994; Yilmaz 2001) this complexity. However, to date there exists no published method to classify observed multiply diffracted wavefields as ordered sequences of diffractors visited, without first estimating a model or representation of the medium (including the diffractors) and then modelling the resulting wave propagation (which we refer to as 'model-based' methods). This is an important omission, not least because many fields of endeavour focus on the wave propagation itself, or on the transmission of encoded signals or information. In principle, such fields may not require knowledge of the model of the medium through which the energy propagates (Prada & Fink 1994; Fink *et al.* 2003), and indeed it may be seen as an advantage if they did not have to rely on model-based methods. Hence, a 'model-free' method to unravel and interpret complex wavefields might find diverse fields of application.

In this paper, we present a method to classify diffractors based on the variation of acoustic wave traveltime variations (their so-called

'moveouts') across arrays of sources and receivers. We show that this information is sufficient to allow the diffraction path of any recorded, multiply diffracted wave to be determined: each recorded wave can be associated with the concatenation of an ordered series of known, irreducible, interdiffractor paths, or equivalently by an ordered series of single-diffractor interactions. These are determined purely by data analysis through inspection and comparison of data from individual sources, and to individual receivers, without the need for synthetic wavefield computation, or for modelling of the medium through which energy propagates.

The method is effected by a new algorithm that identifies diffraction paths by wavefield analysis. Applications of the proposed algorithm within the various fields above range from interpreting reverberating wave energy associated with multiply diffracted waves in terms of the contributions of its individual diffractors, improved location or characterization of diffractors or energy sources, removal of multiply diffracted energy by muting or filtering to improve the performance of methods designed only for singly diffracted energy, and all of these may lead to improved imaging of the interdiffractor medium.

In what follows, we begin by defining what we refer to as a diffractor's 'fingerprint'. Then we introduce a new algorithm to identify diffraction paths. Finally, we present results of applying the algorithm to a synthetic example, before discussing various implications of this work.

2 FINGERPRINTING INDIVIDUAL DIFFRACTORS

A basic geometrical property of all waves diffracted last at a certain diffractor is that their moveout (the difference in their arrival time at different receiver positions: Sheriff 2002) across an array of receivers is invariant (Khaidukov *et al.* 2004). In other words, moving the source or following a different diffraction path up to that last diffractor, can only affect the constant (lag) component of diffracted arrival times observed at an array of receivers, but not their variation or moveout across the array (Fig. 1a). This property holds irrespective of the complexity of the medium, and can be demonstrated rigorously by analysing the fully non-linear Lippmann Schwinger equation for perturbed media (shown in the Appendix). This characteristic of diffracted waves can be used to identify and remove diffraction components, to enhance the diffracted wave signals by removing reflected and refracted waves and to identify edge diffraction signals (Klem-Musatov 1994). By reciprocity, moveout across a source array of all waves diffracted first at a certain diffractor is invariant with respect to receiver position and to the subsequent diffraction path (Fig. 1b). In addition, other than for pathological cases (for example, where diffractors are located exactly symmetrically with respect to (on either side of) straight receiver arrays), each diffractor exhibits a different moveout across source and receiver arrays. Pathological cases only exist when the data are non-directional [e.g. pressure measurements in acoustic media]; when directional measurements like particle velocity or displacement are recorded, moveouts of each diffractor can be discriminated uniquely in all cases and no pathologies exist. Therefore, each diffractor can be 'fingerprinted' or tagged uniquely by their associated moveout, without knowing any diffractor's location. In the following, we discuss how this simple property is sufficient to analyse and identify all diffractors in the path of any particular observed multiply diffracted wave.

3 IDENTIFYING FIRST AND LAST DIFFRACTORS

When multiple diffractors are embedded within an otherwise homogeneous or smoothly varying medium, measured seismograms record direct (non-diffracted), singly diffracted and multiply diffracted waves. Despite their complexity, the path followed by energy in multiply diffracted wavefields can always be decomposed into three subpaths (Fig. 2): a first connecting the source to the first diffractor (dashed line in Fig. 2), a second connecting all of the diffractors involved (solid line in Fig. 2) and a third connecting the last diffractor to the receiver (dotted line in Fig. 2). Notwithstanding the potential complexity of the interdiffractor component, for each source and receiver the possible number of combinations for the first or third of these subpaths is limited and equal to the number of diffractors.

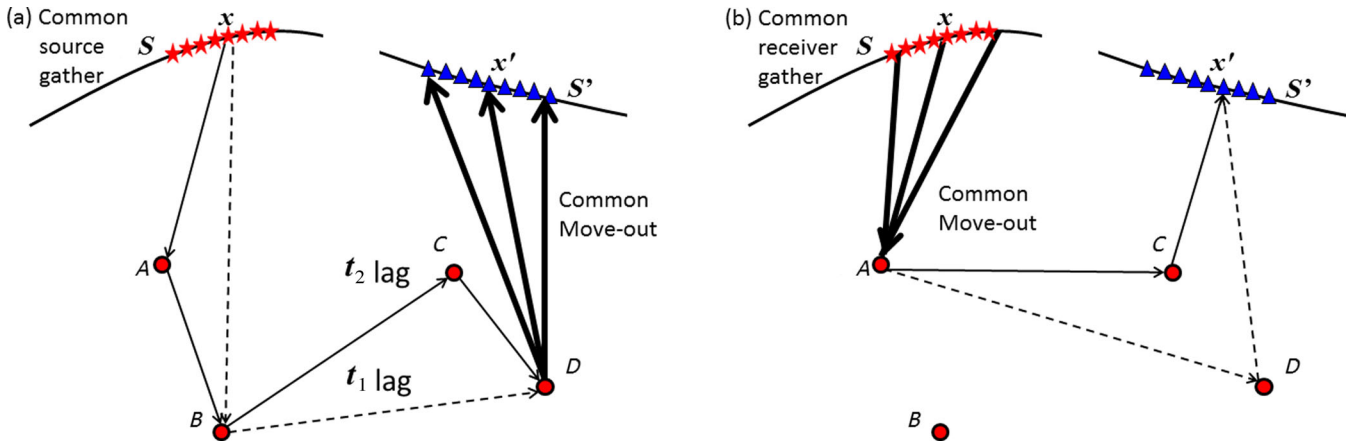

Figure 1. Diffracted wave ray paths. Stars and triangles are sources and receivers, respectively, and circles are diffractors. (a) A fixed source is fired at position x on surface S, and the corresponding wavefield is recorded at receivers at locations x' on surface S'. Arrivals that share identical last diffractor (dashed and solid paths) exhibit the same receiver-array moveout. The receiver-array traveltime variation, or moveout, associated with diffracted waves does not depend on the position of the source since relative traveltime differences are controlled only by the ray paths between the final diffractor and the receivers (bold rays). The traveltime between the source and the diffractor (solid and dashed rays) only changes the constant component of all traveltimes (t_1, or t_2 lags are due to different source positions or diffraction paths). (b) As for (a), but for a fixed receiver: waves that share an identical first diffractor exhibit the same source-array moveout.

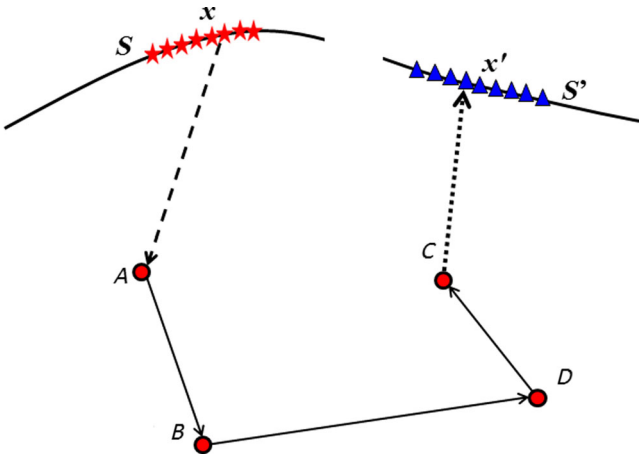

Figure 2. Any multiply diffracted wave can be divided into three subpaths: the source-to-first-diffractor (dashed ray), the interdiffractor path (solid ray) and the last-diffractor-to-receiver path (dotted ray). The complexity of the interdiffractor component (which may also have zero length for a singly diffracted wave) does not affect the simplicity of the first and third components. Symbol key as in Fig. 1.

Since each and every diffracted wave has a first and last diffractor (which may coincide in the case of first-order diffraction), in principle a classification of all diffracted waves can be made based on this information. However, in order to be useful for the analysis of real wavefields, this classification needs to be identifiable from recorded data. We now show how this can be achieved.

Say a source is fired at x, a point on surface S and waveform recordings are acquired at receivers at x' along surface S', where S and S' may differ (Fig. 1a). Among the many diffraction combinations, two paths are shown as solid and dashed thin lines in Fig. 1(a). Both paths have last diffractor D, and therefore exhibit identical moveout across the receiver array (the moveout of the bold ray paths in Fig. 1a). All waves diffracted last at D will share this moveout, and only in pathological cases would any other wave share this moveout. Thus all waves diffracted last at D can be identified and classified as such. A similar classification can be made for every other last diffractor. As a result, in the case that the distribution of receivers on S' is dense enough to identify the moveouts of each diffractor without ambiguity, any diffracted wave can be classified according to its last diffractor.

By reciprocity, a similar argument holds for moveout across the source array on S, and the 'first' diffractor of any diffracted wave can always be identified for any recorded event (Fig. 1b). It is important to note here that the means by which each first and last diffractor are identified is exactly by matching the moveouts in the fingerprint of that diffractor, as introduced in the previous section.

For singly diffracted waves, the first and the last diffractor coincide and the corresponding common-receiver/common-source moveout pairs fully fingerprint the diffractor involved. At no point above or below, do we need to identify where the diffractors are located or any ray paths; we only identify diffractors by their moveout based fingerprints.

In the derivation of the expression for the scattered field in the Lipmann–Schwinger equation, no assumption is made about the background model (see Appendix). This system of classification therefore also extends to diffractors embedded in inhomogeneous backgrounds. It therefore begins to decompose the complexity of wavefields associated with quite a general class of multiple-diffraction problems into more readily identifiable subcomponents.

4 IDENTIFICATION OF FULL DIFFRACTION PATHS

We now present an algorithm that identifies all diffractors involved in the multiple-diffraction path corresponding to any particular observed wave arrival, and their order in the sequence of single diffraction interactions. The ray geometries employed within the algorithm are depicted in Figs 3 and 4. They require only densely sampled distributions of sources and receivers along sections S and S', respectively, of some surface or boundary. Source and receiver density, and the spatial extent of S and S' only have to be sufficient to allow different moveouts to be discriminated, and S and S' need not span the same physical surface.

We first explain the method conceptually, assuming that events in the data corresponding to the rays invoked in each step (namely, first- and second-order diffractions) are known. To foster clarity in the explanation, we draw illustrative, simplified data gathers that only include the diffraction events of immediate interest at each step of the algorithm (Figs 3b, d, f and h). Thereafter, we work through a synthetic example that shows how these particular events can be identified for every ray path in practice, using only recorded data. Note that a gather (in the terminology of exploration seismology, which is useful here) is a subset of a recorded data subset: a common-source gather is the data subset recorded at all receivers for a single, fixed source (which all of those data have in common), and vice versa for a common-receiver gather.

Consider a specific event associated with a source at x_1 and a receiver at x_2 (as indicated by a black star in the illustrative gather of Fig. 3b), and let x_2 be one of the set of receivers on boundary S'. In order to analyse its diffraction path marked as α in Fig. 3(a), we first need to identify its last diffractor (L in Fig. 3a). This information is identified by its unique moveout or fingerprint with respect to the set of receivers. This is indicated by the two identical solid moveouts in 3(b), offset by a constant time-shift: the red corresponds to a first-order event [x_1-to-L-to-x_2], the black to the complete diffraction path α.

Our aim is to identify the full diffraction path. The way our algorithm works is to identify also the penultimate diffractor (L-1), and the recorded energy that corresponds to its 'partial' path [x_1-to-1-to-2-. . . -(L-1)-to-x_2], that is, to path α but omitting the last scatterer L (Fig. 3g). By induction (iterative application of the algorithm to this newly identified energy), this procedure can therefore be used to identify diffractors L-2, L-3, . . . , 1 and thus the full diffraction path α.

To analyse the gather associated with source x_1, we need to introduce an additional source. Let x be this arbitrary source which lies on surface S (Fig. 3c). Step 1 of the algorithm involves subtracting the traveltimes of the wavefield corresponding to the second-order diffraction path [x-to-V-to-L-to-x_2] from that of path α. This is repeated for each of the possible penultimate diffractors V (since at this stage we do not know which one is correct). In Fig. 3 and subsequent figures, traveltimes of waves propagating along dashed rays are subtracted from those along the solid ray paths; hence traveltimes along common solid and dashed ray segments cancel out. When V is chosen to be the correct penultimate diffractor of α as it is in Fig. 3(c), the subtraction of traveltime of the second-order diffraction path [x-to-V-to-L-to-x_2] (this event is indicated by a dashed curve in the illustrative gather of Fig. 3d) results in cancellation of the traveltime of the common segment [(L-1)-to-L-to-x_2], and subtraction of the time along segment [x-to-(L-1)] from the traveltime for the remainder of path α. Note for later that if V is not the penultimate diffractor then the result of this

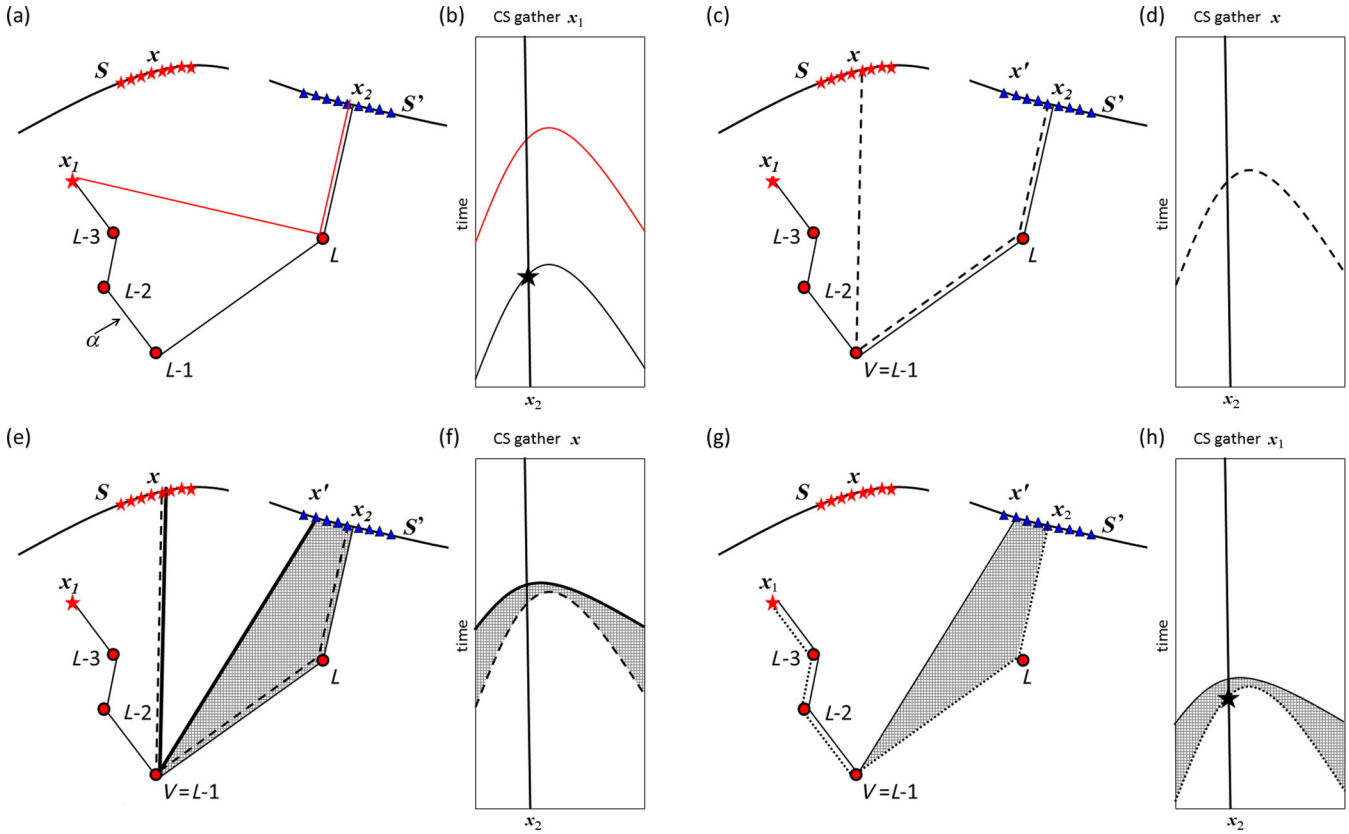

Figure 3. Schematic representation of the geometry required to identify all diffractors in a wave path. Symbol key as in Fig. 1. (a) A recorded multiply diffracted arrival corresponds to a source at some location x_1, recorded at any receiver x_2 (black star in b) that is part of a set of receivers along section S' of a surface. The final diffractor, L, is uniquely identified by its moveout with respect to these receivers (as indicated by the repetition of the same moveout as the primary, red curve in the illustrative gather in b, corresponding to source x_1). (c) Step 1 of the algorithm involves subtraction from the traveltime of the multiply diffracted arrival in (a) of the time of the second-order diffracted energy corresponding to the path [x-to-V-to-L-to-x_2] (dashed curve in the illustrative gather corresponding to source x, shown in panel d). Here, x is an arbitrary source on S. The procedure to identify second-order diffracted waves (the dashed ray in c) is explained in Figs 7–9. (e) The third step of the algorithm involves addition of the previous result with the traveltime of the first-order diffracted energy (or fingerprint) corresponding to the path [x-to-V-to-x'] where x' is an arbitrary receiver on S' (bold solid line in the illustrative gather corresponding to source x, in f). For our synthetic examples below we have chosen $x' = x_2$, but this is not necessary as both x_2 and x' can be varied arbitrarily across the receiver array. (g) If and only if $V = (L\text{-}1)$, that is, V is chosen to be the penultimate diffractor of the multiply scattered path in question, then the result of the previous operation provides the traveltime of an arrival with the kinematics of physical, observed energy in the original seismogram from the source at x_1 recorded at x' as shown, for all x' on S' (as indicated by the solid line in the illustrative gather corresponding to source x_1 in panel h); thus the penultimate diffractor V = (L-1) is identified. Note that moveout difference in (f) is the same as in (h).

operation has a more complex geometrical interpretation as shown in Fig. 4.

The result of this operation is then added to the traveltime of the primary diffracted wave [x-to-(V)-to-x'] (solid bold lines in Figs 3e and f), x' being the location of any arbitrary receiver on surface S'. As illustrated in Fig. 3(e) and shown below, if and only if V is the penultimate diffractor of α (i.e. $V = L$-1) then the above set of operations reproduces the traveltime of a real wave travelling along the partial path [x_1-to-1-to-2-. . . -(L-1)-to-x'], that is observed in the recorded data at receiver x', for all x' on S' (Figs 3g and h). The main result expressed in Fig. 3 is therefore that the difference between the traveltimes of any multiply diffracted wave and another diffracted wave following the same path but omitting the last diffractor (Fig. 3g) is controlled by the difference between the traveltimes of a primary diffracted wave [involving the penultimate diffractor (Fig. 3e)] and a twice-diffracted wave [involving the penultimate and the last diffractor (Fig. 3e)]. This is shown by the difference (shaded areas) between the moveouts in Fig. 3(f), which is demonstrably the same difference as that in Fig. 3(h), and this is true for any intermediate source x used in Fig. 3(e).

Crucially, if we have chosen V to be the correct penultimate diffractor (L-1), we should be able to *observe* physical energy in the wavefield recorded along S' from source x_1 at the traveltimes predicted by the above sequence of steps. If instead of $V = L$-1 we had used energy associated with any other penultimate diffractor (e.g. $V = L$-3 as shown in Fig. 4), the above procedure would not have produced an arrival time or moveout of a real wave, and hence its energy would not have been observed in the recorded data at those times. Thus that choice of diffractor for V can be ruled out. Conversely then, the presence of energy on the recorded seismograms corresponding to source x_1 that matches the traveltime and moveout across receivers x' on S' predicted as above, allows the penultimate diffractor $V = L$-1 to be identified.

By induction, all diffractors on path α may be identified similarly: the algorithm is simply iterated to identify the penultimate diffractor of the newly identified energy associated with the partial path [x_1-to-1-to-2-. . . -(L-1)-to-x'] in Figs 3(g) and (h) which is physically observed in the recordings at any x' on S' and hence also at x_2. Since the diffractors are thus identified in exactly reversed order, the

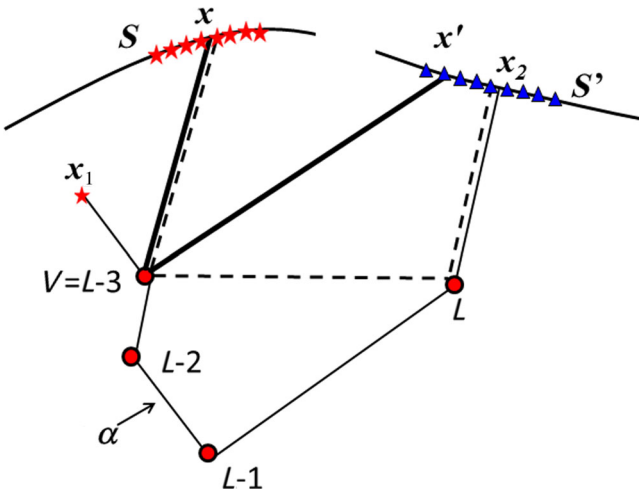

Figure 4. If in the second step of the algorithm depicted in Fig. 3(e), a diffractor V is chosen that is not the penultimate diffractor on path α, the result of applying the algorithm will be the time of [x_1-to-1-to-2-to-. . . -to-(L-1)-to-L], plus that of [V-to-x'], minus that of [L-to-V] (traveltimes of path segments [V-to-x] and [L-to-x_2] cancel). The resulting traveltime will not match that of any recorded energy as the result will not have a physical traveltime. Key as in Fig. 3.

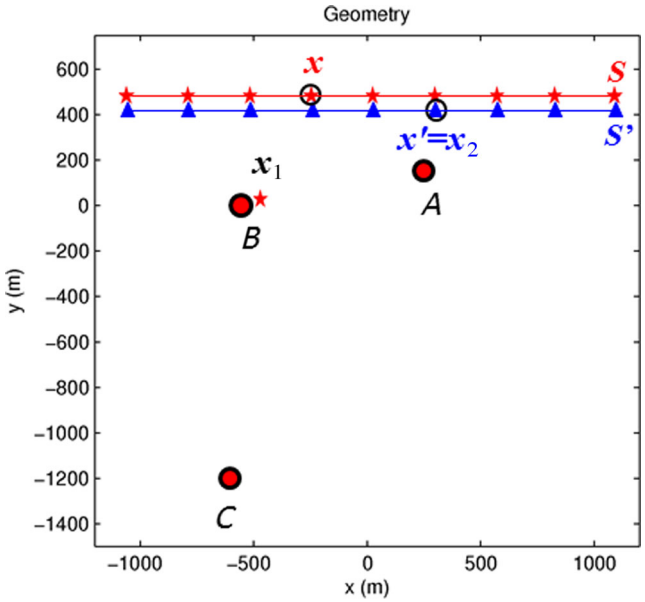

Figure 5. Geometry of the model used in numerical examples. Key as in Fig. 1. A total of 160 sources and 400 receivers are employed in horizontal arrays (only every 20th source and fifth receiver are plotted for clarity). The 60th source and the 190th receiver (used in Fig. 7) are highlighted by circles.

order that diffractors are encountered by the original energy along diffraction path α is revealed.

Despite the fact that the method is applied iteratively, note that in principle no error is accumulated since each iteration is driven entirely by newly identified, physically observed energy diffracted from the penultimate diffractor of the previous iteration. The only error that could be propagated would be a complete misidentification of the predicted energy of path [x_1-to-1-to-2-. . . -(L-1)-to-x'] in the observed data at receivers x' in Fig. 3(g). In principle, such errors can be avoided by using suitably dense and extensive source and receiver arrays on S and S', respectively.

In the above we assumed that energy associated with all first and second-order events could be identified as and when needed. In the next section, we show how the appropriate events can be identified in recorded data sets.

5 WORKED EXAMPLE: IDENTIFICATION OF FULL MULTIPLY DIFFRACTED WAVE PATHS

We now apply the diffraction path identification method presented above to 2-D acoustic synthetic data. We show how the method works as a step-by-step algorithm, and test whether energy is observable in the recorded data at the sums or differences of traveltimes thus predicted. We compute wavefields with a numerical implementation of the Foldy method (Foldy 1945; Groeneboom & Snieder 1995) made available by (Galetti *et al.* 2013). This method is particularly useful for our purposes because it does not suffer from shortcomings usually associated with finite difference modelling tools (i.e. numerical dispersion, spurious reflections from imperfectly absorbing boundaries contaminating later times, etc.). It is also consistent with the acoustic optical theorem which determines the correct values of all scattering amplitudes such that energy is conserved (Groeneboom & Snieder 1995; Snieder *et al.* 2008). Calculations are performed in the frequency domain, but for ease of interpretation we present results in the time domain. A Ricker wavelet with central frequency of 30 Hz is used to generate all wavefields.

We consider a background velocity of 1000 m s^{-1}, a unit density and three isotropic diffractors, with 160 sources and 400 receivers located on horizontal portions of boundaries S and S', respectively (Fig. 5). For each source along the boundary, data are recorded at all of the receivers. The data from surfaces of sources and receivers are then organized into a data 'cube', with each cross-section of the cube corresponding to a common-source or common-receiver gather (Fig. 6).

Any multiply diffracted wave may be characterized by its diffraction path, and the set of all diffraction paths can be classified into subsets of events that share the same 'first' and 'last' diffractors. This can be achieved based on their observed moveouts or fingerprints as described above. In the following example, we analyse the diffracted waves in the trace associated with the source–receiver pair [source x_1, receiver 190] (vertical black line in Fig. 7a).

Three different moveouts are identified (in this case by visual inspection) on each of these gathers (marked A, B and C in Fig. 7a), and each moveout constitutes the common-source fingerprint of an individual diffractor. We conclude that three diffractors are present in the model. As discussed above, the method requires that we identify all first and second-order diffraction events in common-source and common-receiver gathers for an arbitrary source–receiver pair (x', x). Therefore, in order to apply the algorithm for this specific example, a total of three primary and six secondary arrivals must be identified in the data cube, and some of these waves are depicted in Figs 7(b) and (c).

To apply the algorithm to analyse the diffraction path α of some target event (a particular arrival with an observed moveout), we proceed as follows:

(1) Identify all of the primaries. In general, primaries are simply the observed arrivals with the shortest traveltime for any particular common-source gather moveout. Here, we choose to identify the primary in the common-source gather corresponding to x = source 60 on S (see Fig. 7b), but any other source could be used for x. In

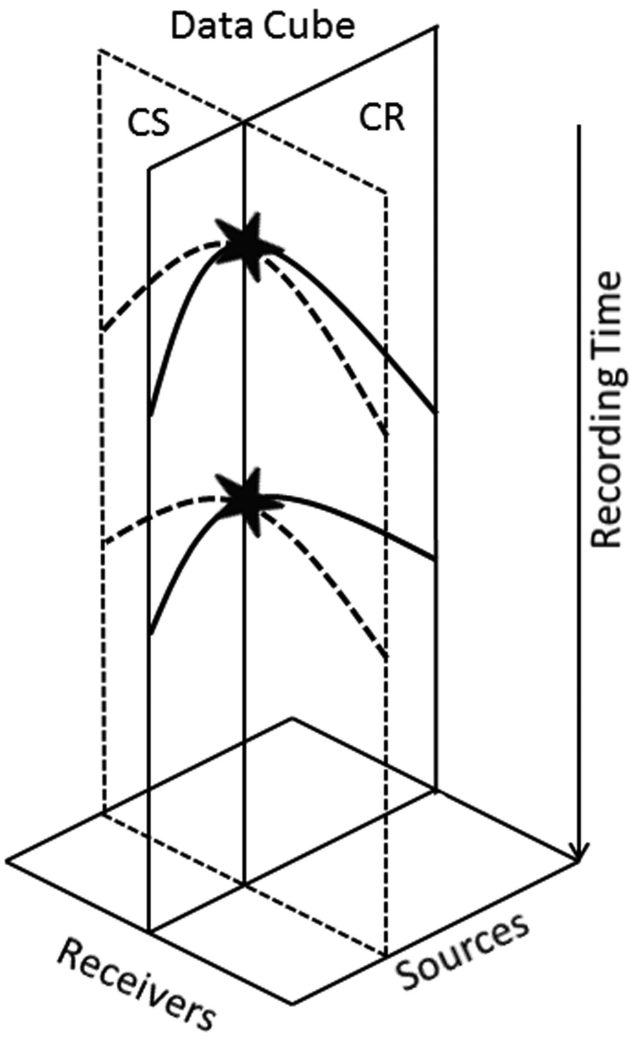

Figure 6. Schematic representation of a source/receiver gather data 'cube' where recorded time-series are organized to be vertical in recording time. Slice CR corresponds to a fixed receiver and hence is a common-receiver gather, while slice CS at a specific source is a common-source gather. At the intersection of these slices, all arriving energy must coincide (stars in the cartoon) because the recorded trace corresponds to the same source–receiver pair in both slices. Thanks to this continuity property it is possible to identify which source and receiver moveouts correspond to the same wave arrivals (pairs of solid and dashed moveout curves in the picture).

Fig. 7, for example, we focus on a single diffractor (i.e. on a single moveout), namely *A* in Fig. 7(a), and its primary is identified by visual inspection as it exhibits the shortest traveltime corresponding to that moveout.

(2) Determine the full common-source/common-receiver single-scattering fingerprint of each scatter by comparing common-source and common-receiver gathers. Arrivals on common-source and common-receiver gathers always converge at one point (Fig. 6), and when involving primaries this allows us to link the common-source and common-receiver moveouts associated with each individual diffractor. All diffractors are then labelled or tagged by their fingerprints. It is important to note again that we thus do not need to locate a diffractor; we can nevertheless label each one uniquely. In the following, we use fingerprint(S, S', F) to refer to the fingerprint of diffractor F defined by moveouts across source surface S and receiver surface S'.

(3) Identify all of the secondary diffracted arrivals for an arbitrary boundary source–receiver pair (x', x). Secondaries are simply identified by finding shortest traveltime pairs of common-source and common-receiver moveouts that are not both in the same fingerprint FP(S,S',F) of any one diffractor F (see Figs 7b and c, 8b and c and 9b and c) and that therefore are associated with pairs of first and last diffractors.

(4) Identify in the data (e.g. in Fig. 7a) the same traveltime differences between pairs of moveouts as is observed between the moveouts of second and first-order diffraction events (depicted at either end of the braces in Figs 8–10b). For any pairs of events in the recorded data that are found to have the same moveout difference as that observed between a secondary and a primary, the last and penultimate diffractors can be determined to be the same as those involved in that secondary and primary. For example, the arrows between Figs 7(e) and (d) show how to identify such pairs of moveouts of events that must share the same last and penultimate diffractors.

(5) Label each pair of events identified in step 4 as having the same last and penultimate diffractors as those of the corresponding first and second-order diffractions.

(6) For the target event, in step 5 one other moveout will have been labelled as being from the same path α as the target event except that it diffracted last at the penultimate diffractor, that is, it comes from the partial path that omits the final diffractor.

(7) Redefine the target event as the event associated with the penultimate diffractor, and redefine the target path α as the corresponding partial path.

(8) Repeat the analysis from step 4 to the new target event, until the new target event is one of the primaries labelled in step 2.

(9) Concatenate the labels of all of the last diffractors (identified by the common-source gather moveouts) of target events used in each iteration, and reverse their order. Thus we identify the labels of all diffractors involved in the full diffraction path of the original target event.

Fig. 10 shows the seismogram along the bold line in Fig. 7(a) along with the diffraction paths associated with most of its multiply diffracted waves as identified by the algorithm. This represents the final result of applying the method herein. We use *C–B–A* as notation to indicate energy that visited diffractors *C* then *B* then *A* before being recorded. A total of five second-order, five third-order and one fourth-order diffracted waves were able to be identified in this example.

To illustrate how the algorithm is applied, we arbitrarily show how to decompose the target arrival occurring at 4.5 s in Fig. 10 (along the bold line in Fig. 7a) into a corresponding ordered sequence of diffractors (the target path) visited by that wave energy. All other arrivals in Fig. 10 were analysed similarly to identify all diffraction paths shown on that figure.

First, we identify the last diffractor. This is readily provided by matching the moveout of the target arrival on the common-receiver gather in Fig. 7(a) with the fingerprint of one of the diffractors identified above. In this case, the wave has the same moveout as the primary corresponding to diffractor *C* (see Fig. 9b), making that the last diffractor of the target path.

The penultimate diffractor can then be either diffractor *A* or *B*; to identify which, we proceed as shown in Figs 3 and 4. As indicated in Fig. 3, the traveltime difference between the diffracted wave corresponding to any diffraction path and the same generic path without the last diffractor (Fig. 3g), is controlled by the difference between a primary (involving the penultimate diffractor) and a secondary wave (involving the penultimate and the last diffractor—Figs 3e

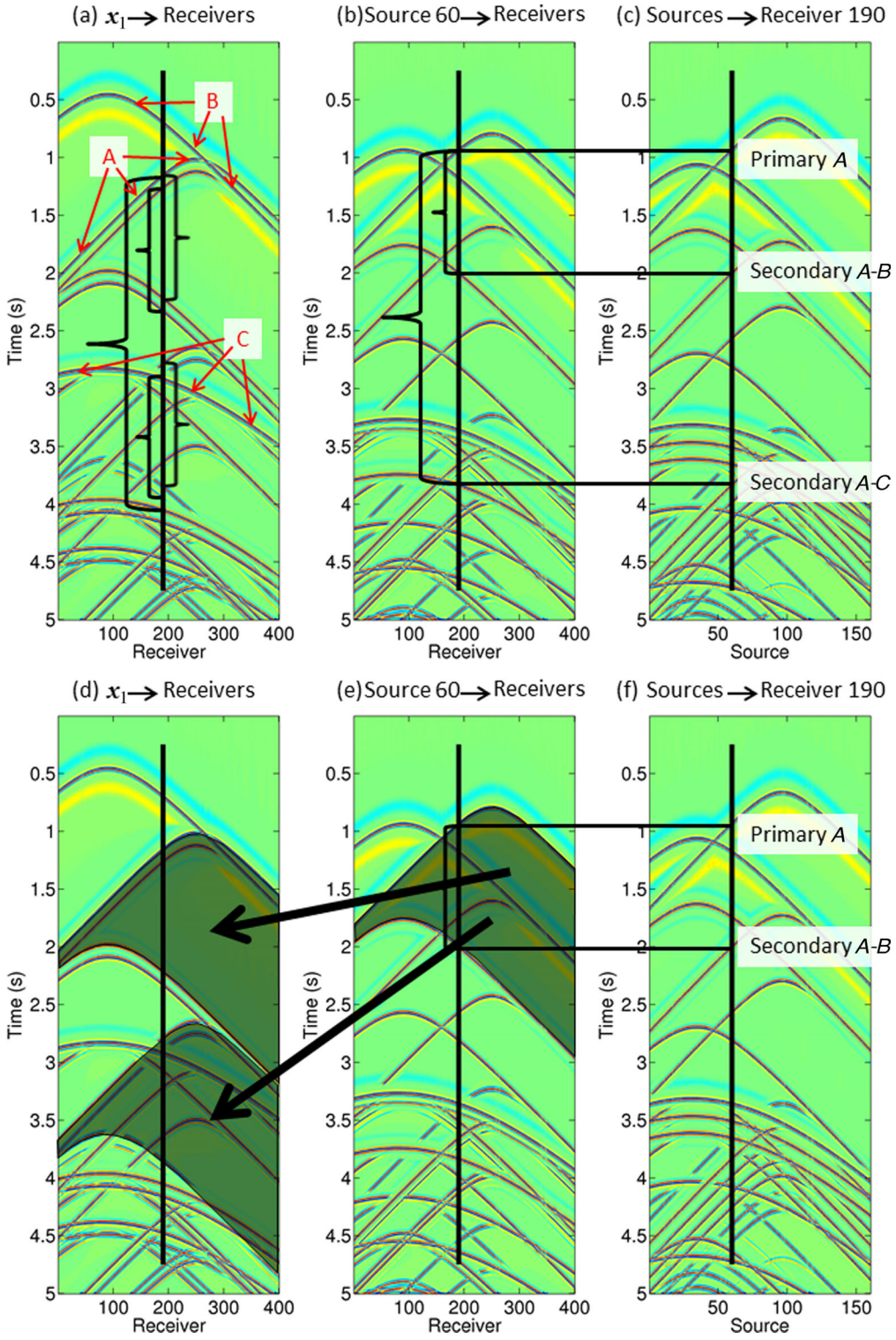

Figure 7. Temporal waveforms (or traces) for the experimental geometry in Fig. 6. (a) Common-source gather for source x_1 of Fig. 5, and (b) similarly for the 60th source. In (a), arrivals *A*, *B* and *C* exhibit three distinct moveouts, thus indicating that there are three distinct diffractors. The vertical black line indicates the 190th receiver x' of Fig. 5. (c) Common-receiver gather for the 190th receiver in Fig. 5. The vertical black line indicates the 60th source x of Fig. 6 for which (b) shows the common-source gather. The vertical black lines in (b) and (c) indicate the same signal corresponding to source number 60 and receiver 190 where panels (b) and (c) must coincide by reciprocity (Fig. 6), thus identifying common-source and common-receiver primary moveout pairs (fingerprints) for each of the diffractors. Black braces indicate traveltime and moveout differences between primary and secondary diffraction energy—annotated numbers indicate the individual diffractors involved. (d)–(f) as for (a)–(c), but showing the occurrence of identical moveout pairs as difference intervals instead of braces (only two surfaces are shown for readability purposes). A gain has been applied to all waveforms progressively in time to enhance the signal corresponding to long and multiply diffracted paths. Mutual interference of traces can occur, especially in the latter portions of recorded signals. However, often the visible presence of only a fraction of a moveout curve is sufficient to discriminate it from others. The direct wave has been removed from all of the gathers to foster readability. Note that despite the proximity of source x_1 and diffractor *B* (see Fig. 5), direct and diffracted waves are clearly separable.

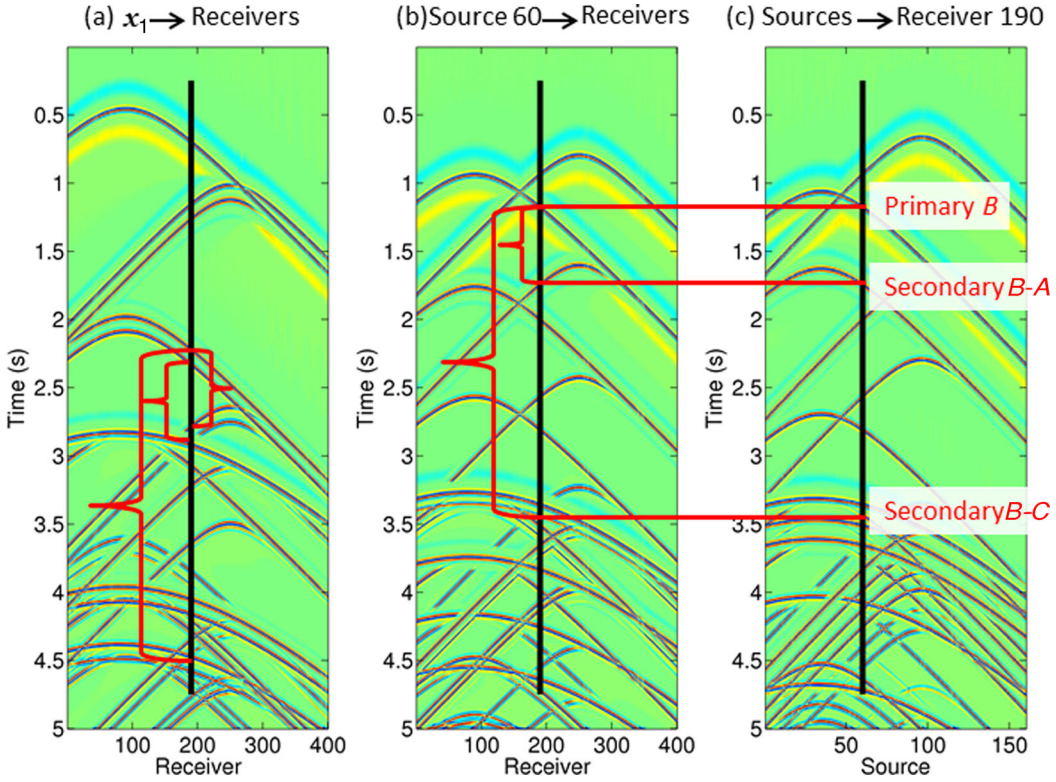

Figure 8. As for Figs 7(a)–(c), but for first scatter *B* in Fig. 5 (identified by a different fingerprint). Braces are red to indicate that a different primary diffracted wave is being analysed compared to Fig. 7.

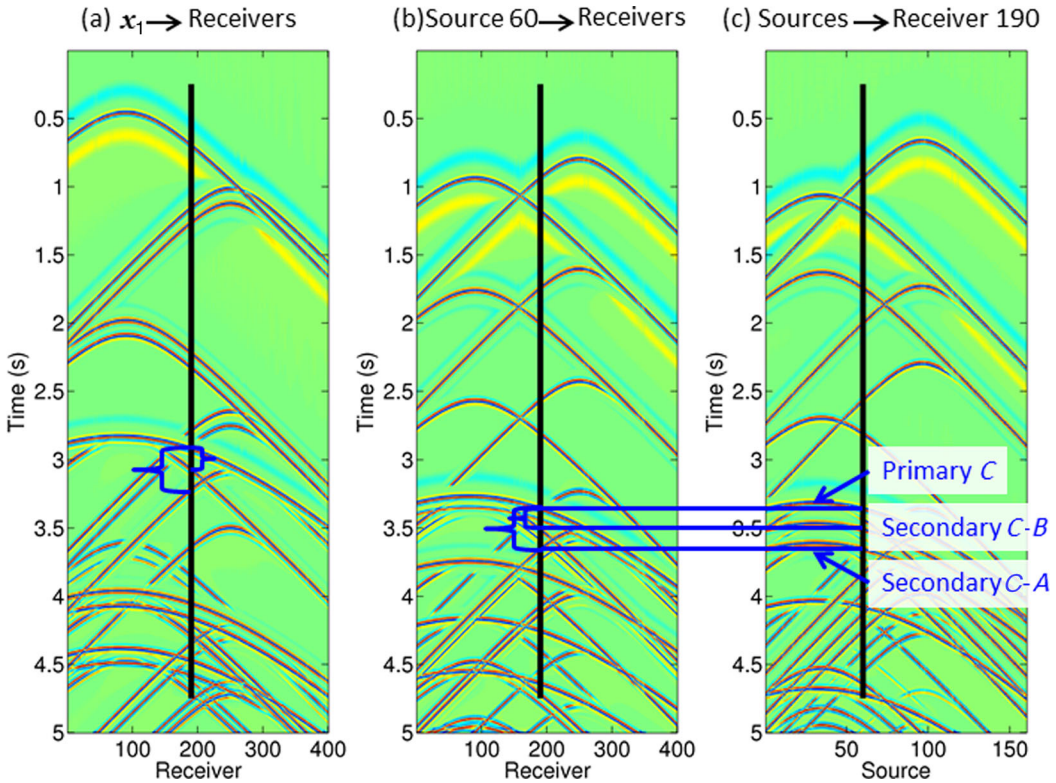

Figure 9. As for Figs 7(a)–(c), but for first scatter *C* in Fig. 5 (identified by a different fingerprint). Braces are blue to indicate that a different primary diffracted wave is being analysed compared to Figs 7 and 8.

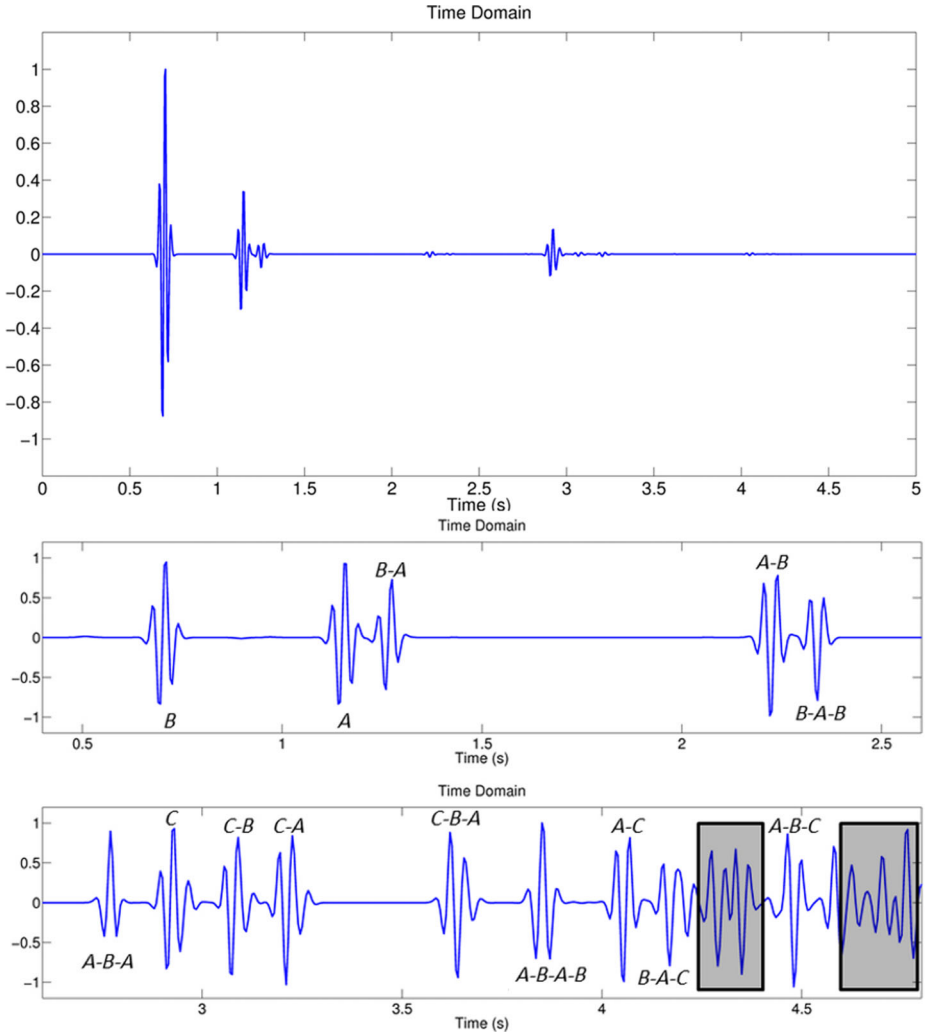

Figure 10. Top plot: the waveform along the vertical bold line in Fig. 7(a), with no gain applied. Middle and lower plots: the sequence of diffractors involved in each arrival as obtained by the new algorithm is shown by letters A, B and C in the order in which diffractors were encountered (each panel shows a different portion of the top waveform). Only some very low amplitude, overlapping arrivals (e.g. in the shaded boxes, lower plot) were not able to be analysed due to difficulties in moveout discrimination. A gain has been applied to the lower plots for better readability: this operation has rescaled each event relatively to the others.

and f). More precisely, once the difference between the correct secondary and primary traveltimes is subtracted from the traveltime of the target arrival, the result should be the traveltime of a new wave that is also actually observed in the seismogram, for any and all receivers across the array.

Since *a priori* the penultimate diffractor is not known, we calculate the above differences for all potential penultimate diffractors. When the correct one is chosen, the result matches observed energy across the entire receiver array. On the other hand, for all incorrect penultimate diffractors this operation will not match observed energy across the array, provided the array is sufficiently extensive to discriminate.

We therefore compare the traveltime differences between the secondaries A–C and B–C, and the primaries corresponding to diffractors A and B, respectively, from (arbitrary) surface source 60 (shaded intervals in Figs 11b and d, respectively), and the observed data from the original source at x_1 (Figs 11a and c, respectively). Only when the correct penultimate diffractor (in this case, diffractor B) is used, do the relative moveout pair differences match a difference observed in the original data. This is indicated by solid arrows in Figs 11(a) and (b). In all the other cases, no energy corresponds to the expected traveltimes, as indicated by the dashed arrow between Figs 11(c) and (d): the top arrow between the latter plots points at a location in Fig. 11(c) at which there is no observed energy. Thus, we reject C as the penultimate diffractor of the target path.

Once the penultimate diffractor has been determined, the same procedure is repeated but starting with the newly identified energy, observed as indicated by the top arrow in Fig. 11(a), at $x' = x_2$. Thus, the penultimate diffractor of the previous iteration becomes the last diffractor of the current iteration, and therefore different observed primaries and secondaries are used in the algorithm. The procedure ends once one of the (previously identified) singly diffracted waves is reached. This is illustrated in Fig. 12, in which diffractor C is identified as the penultimate diffractor of the path of the 'new' energy identified by the top arrow in Fig. 11(a). The target diffraction path has thus been identified as A–B–C and is added to Fig. 10 above the arrival at 4.5 s.

The procedure is repeated, treating each of the other arrivals in Fig. 10 in turn as target arrivals. Thus, we obtain all diffraction paths described in that figure.

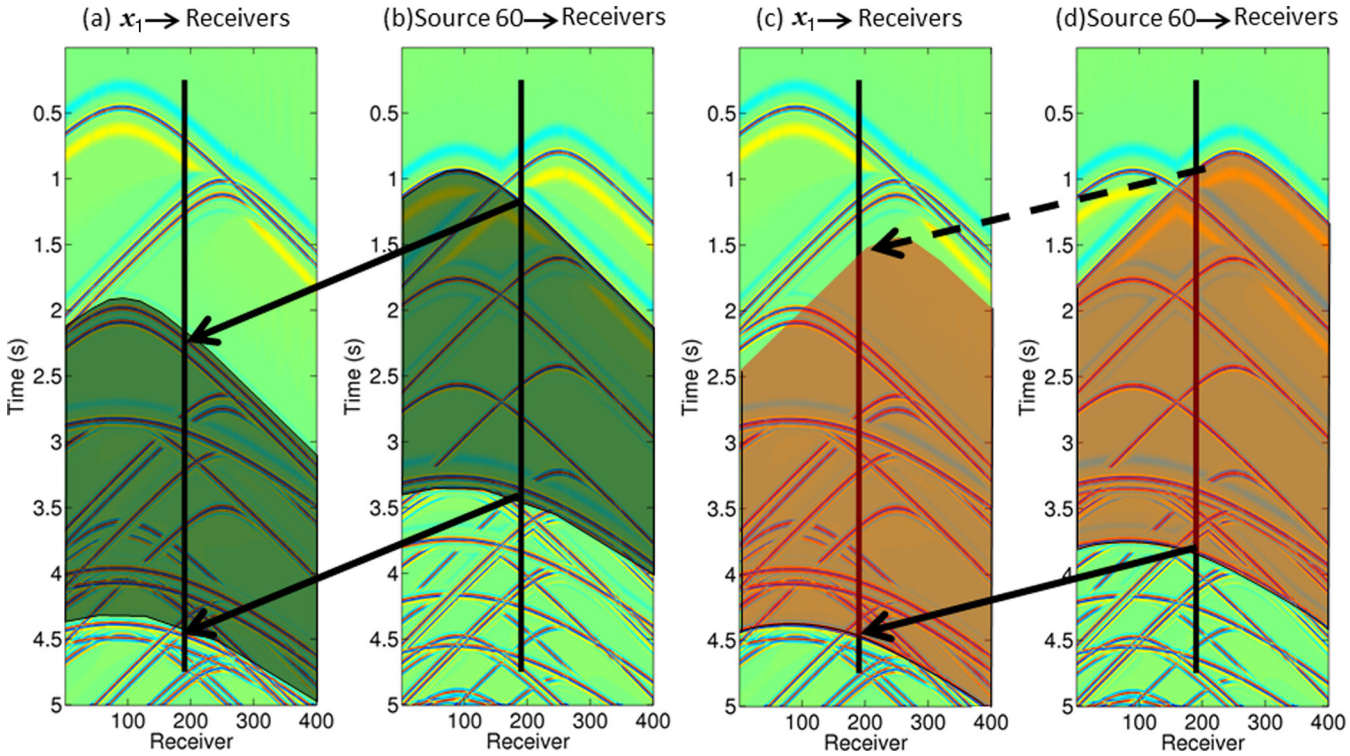

Figure 11. Analysis of the diffracted wave arrival at ∼4.5 s along the bold line in (a). An identical moveout pair sequence is shared by the observed data in (a), and the arrival time difference between primary (*B*) and secondary (*B*–*C*) in (b), as shown by the solid arrows and upper boundary of the black shaded area that match observed energy in (a). This identifies the last (*C*) and penultimate (*B*) diffractors associated with the arrival observed at ∼4.5 s. An identical moveout pair sequence is not shared by the observed data (c) and the difference between primary (*A*) and secondaries (*A*–*C*) in (d), as shown by the dashed arrow and upper boundary of the red shaded area that does not match observed energy in (c). This excludes *A* as the penultimate diffractor for the arrival observed at ∼4.5 s.

6 DISCUSSION

In principle, diffracted waves can be used profitably in geophysics as they provide information about spatially abrupt boundaries like faults, voids rough topography or subsurface layers, etc. In addition, discrimination, identification, analysis, and in some cases removal of singly- or multiply diffracted waves can help to enhance desired signals or to suppress unwanted 'noise' in recorded data. Similar benefits exist in the other fields of application identified in the introduction.

The proposed algorithm to identify full diffraction paths is based on diffractor fingerprints, so-called by analogy with the virtually unique identifiers of humans. Here, the identifiers are moveouts of primary (singly scattered) arrivals across arrays of sources or receivers. In the example presented above, the algorithm was implemented manually, that is, the different moveouts were identified and matched to other moveouts by visual inspection. In the ideal condition of noise-free data considered here, this allowed up to fourth-order diffracted waves to be identified fairly easily.

The robustness of the method was not evaluated in terms of, for example, its sensitivity to temporal and spatial resolution of the recorded data, which may affect the identification of different moveouts (Meles & Curtis 2013b). It is presumed that the efficacy of the overall procedure will be affected by these and other aspects (e.g. different signal-to-noise ratios, the number and distribution of the diffractors, heterogeneities in the interdiffractor background velocities, etc.). More specifically, all these factors may affect the ability to extract first and second-order diffracted events, and therefore impede full application of the algorithm: it is clear from the gathers shown in Figs 7–9 that it would be trivial to add sufficient synthetic noise such that the human eye could not identify, for example, moveouts of later arriving energy. Nevertheless, it is also clear that for low noise, and strongly diffracted energy, the algorithm would be expected to identify some multiply diffracted energy in such data.

One of the strengths of the algorithm is that it is based purely on the kinematics of recorded energy; that is, it only involves subtraction and summation of 'traveltimes' of multiply diffracted waves. For this reason, the method could also be applied to dissipative background media and diffractors, as it does not rely on amplitude information at all. However, it may also be possible to generalize the method to include dynamic wavefield information (e.g. amplitudes). This might be achieved by employing cross-correlation and convolution of the various recorded diffracted wave arrivals in place of subtraction and summation of their traveltimes within the algorithm. In so doing, we actually apply the trilinear source–receiver interferometry (SRI) operator of Curtis & Halliday (2010), Meles & Curtis (2013a,b) and Löer *et al.* (2013) to the data. Such operators are generally used for wavefield synthesis (as in Curtis & Halliday 2010) rather than analysis (as above), and for the specific geometry considered here with S and S' only spanning one side of the medium, we would construct only an approximation to the true multiply diffracted energy between x_1 and x_2 (Meles & Curtis 2013a,b). The method herein thus shows how the same SRI trilinear operators can be used for wavefield analysis rather than synthesis, and also sheds light on the internal workings of such operators, and how they combine information contained in (multiply) diffracted energy [see also King & Curtis (2012) and Löer *et al.* (2013)].

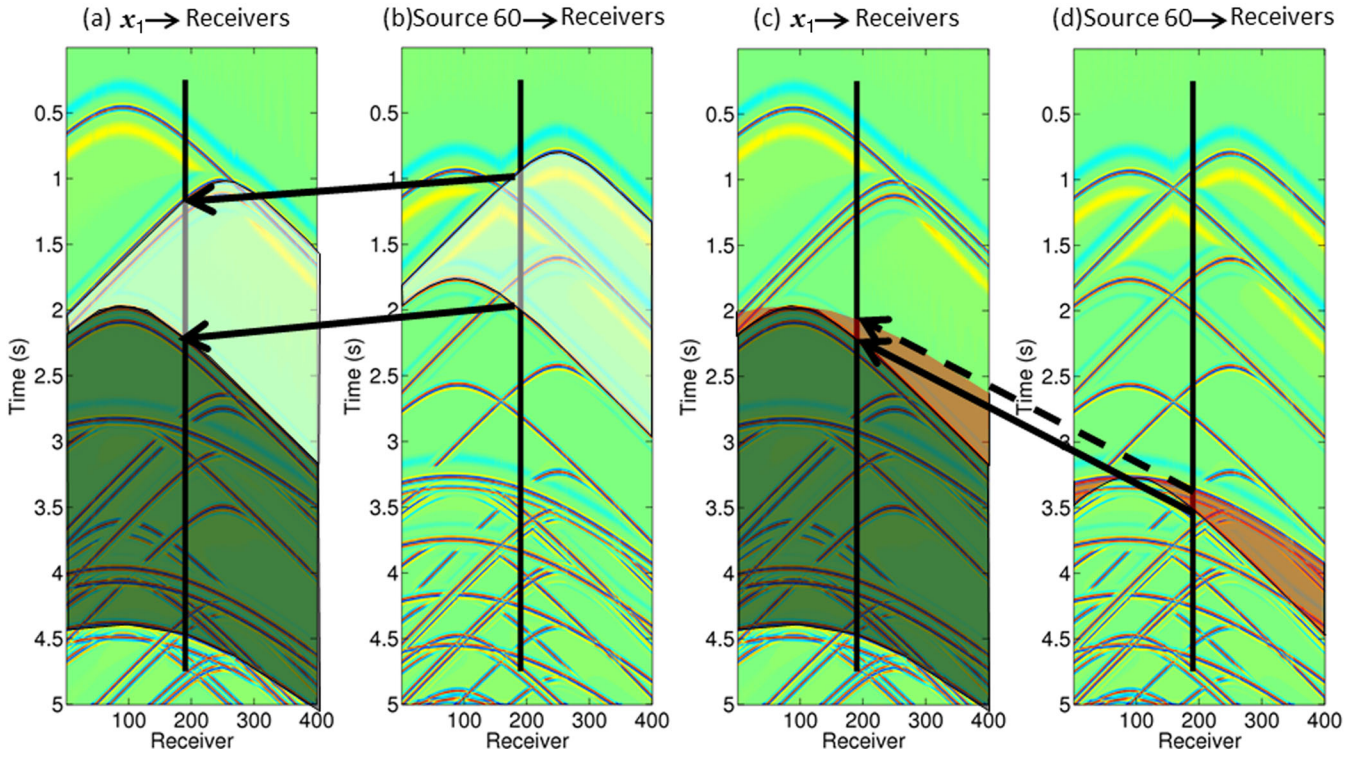

Figure 12. (a)–(b) As for Figs 11(a) and (b), but for the wave arrival at ∼2.25 s along the bold line in (a) identified in Fig. 11 as corresponding to the penultimate diffractor. An identical moveout pair sequence is shared by the observed data (a), and the arrival time difference between primary (*A*) and secondary (*A*–*B*) in (b), as shown by the solid arrows and upper boundary of the white shaded area that match observed energy in (a). This identifies the last (*B*) and penultimate (*A*) diffractors associated with the arrival observed at ∼2.25 s. Since the algorithm now involves a primary as the wave associated with the penultimate diffractor (see (a)), the complete diffraction path has been identified. (c)–(d) As for Figs 11(c) and (d): a moveout pair sequence that is not shared by the observed data and the difference between primary (*C*) and secondary (*C*–*B*), as shown by the dashed arrow and upper boundary of the red shaded area, does not match observed energy in (c). This excludes *C* as the penultimate diffractor for the arrival observed at ∼2.25 s.

In practical applications, the method may itself provide valuable information about interdiffractor medium properties, which could be analysed by comparing amplitudes or phase variations between differently singly and multiply diffracted waves. This is illustrated for example in Fig. 13, which shows how the traveltime 'between two diffractors' can be evaluated by subtracting half the traveltimes of zero offset (x_1–A–x_1 and x_2–B–x_2) first-order diffracted energy from the traveltime of second-order diffracted event (x_1–A–B–x_2). Since all of these events are identified by their diffractors in the algorithm above, observing the traveltime of interdiffractor path [A–B] is trivial for all pair of diffractors.

In a physical experiment, Fink *et al.* (2003) proved that the energy from singly and multiply diffracted waves recorded across a transducer array could be refocused on their last diffractors through exact time-reversal mirroring (by simultaneously emitting the recorded energy, time-reversed, by the same transducers that recorded the energy). In imaging by migration, the same process is simulated on a computer. However, for imaging to work, the corresponding simulated source wavefields also need to arrive at each scatterer at the same time as the refocused time-reversed energy. The source wavefield then clearly needs to account for the multiply diffracted paths that occurs before energy arrives at the last diffractor (Fleury & Vasconcelos 2012; Ravasi & Curtis 2013). Since we can now identify both singly and multiply scattered energy, and the scatterers visited by each arrival, analysis and comparison of different focusing images associated with such waves should provide valuable information on velocity errors in the corresponding interscattering background model, and more generally about its missing diffractors (Sava *et al.* 2005; Coimbra *et al.* 2013).

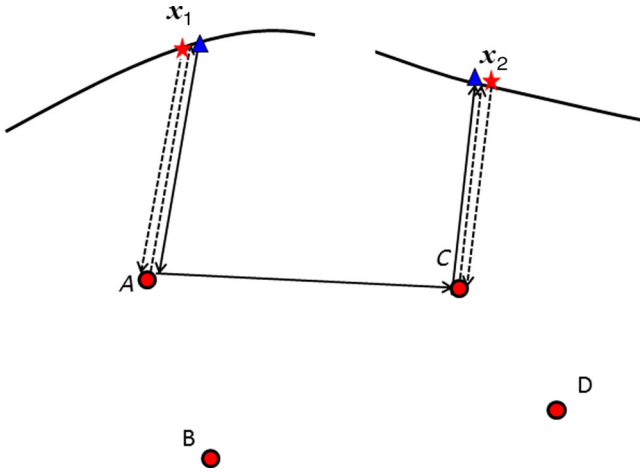

Figure 13. Comparison of zero offset primary (dashed arrows) and secondary (solid line) ray paths sharing identical sections of paths ([x_1-to-A] and [C-to-x_2]) can provide valuable kinematic and dynamic information about interdiffractor paths. The diffraction path identification algorithm proposed here identifies the primary and secondary diffracted energy sharing identical sections of path, thus also identifying the effects of the interdiffractor section of the path A-to-C.

Diffractors are generally characterized by a variety of properties, for example, spatial position and scattering amplitudes

or cross-sections (Groeneboom & Snieder 1995; Wapenaar *et al.* 2010). Multiply diffracted waves are affected by these properties in both phase and amplitude. If we know which diffractors were encountered by each wave, then one may be able to constrain or investigate such properties. For example, in the case that illumination is only provided by limited arrays of sources and receivers, scattering anisotropy could be studied by considering multiply diffracted waves, which may illuminate diffractors from otherwise inaccessible directions.

To our knowledge, this is the first published method to decompose multiply diffracted paths into their individual, ordered, single-scattering components without using an explicit model of the interior of the medium. In this paper, we present a method based on wavefield analysis: that is, we begin with any arrival observed in a waveform and show how it can be analysed to determine the scattering interactions that lead to that observed arrival. Note that Fig. 4 can also be used in reverse, to 'synthesize' multiply diffracted wave traveltimes. That is, the traveltime of the multiply diffracted arrival ending at L-1 in Fig. 3(g) can be added to the traveltime of the dashed secondary diffraction path in Fig. 4(e), then the traveltime of the primary in Fig. 3(e) can be subtracted from the result. This provides the traveltime of a true multiply diffracted wave that should be observed at x_2, and which diffracted last at L as shown in Fig. 3(g). Thus we identify a recorded arrival which has experienced an order of scattering that is one higher than that injected into such an algorithm. In either case, diffraction path identification has been shown to be possible using relatively straightforward deterministic algorithms, and without requiring a model of the medium.

ACKNOWLEDGEMENTS

We are grateful to the Edinburgh Interferometry Project (EIP) sponsors (ConocoPhillips, Schlumberger, Statoil and Total) for supporting this research. We also thank Erica Galetti for providing the Foldy wavefield modelling code and Katrin Löer for insightful comments. The authors thank Xander Campman and an anonymous reviewer for their comments, which greatly helped to improve the paper.

REFERENCES

Bansal, R. & Imhof, M., 2005. Diffraction enhancement in prestack seismic data, *Geophysics,* **70,** V73–V79.

Blomgren, P, Papanicolaou, G. & Zhao, H.K., 2002. Super-resolution in time-reversal acoustics, *J. acoust. Soc. Am.,* **111,** 230–248.

Chadan, K. & Sabatier, P., 1979. *Inverse Problems in Quantum Scattering Theory,* Springer-Verlag, 361 pp.

Coimbra, T., Figueiredo, J.J.S., Schleicher, J., Novais, A. & Costa, J.C., 2013. Migration velocity analysis using residual diffraction moveout in the poststack depth domain, *Geophysics,* **78,** S125–S135.

Curtis, A. & Halliday, D., 2010. Source-receiver wave field interferometry, *Phys Rev E,* **81,** 046601-1–046601-10.

de Figueiredo, J.J.S., Oliveira, F., Esmi, E., Freitas, L., Schleicher, J., Novais, A., Sussner, P. & Green, S., 2013. Automatic detection and imaging of diffraction points using pattern recognition, *Geophys. Prospect.,* **61**(Suppl. 1), 368–379.

de Vries, D. & Berkhout, A.J.., 1984. Velocity analysis based on minimum entropy, *Geophysics,* **49,** 2132–2142.

Dell, S. & Gajewski, D., 2011. Common-reflection-surface-based workflow for diffraction imaging, *Geophysics,* **76,** 187–195.

Derode, A., Roux, P. & Fink, M., 1995. Robust acoustic time reversal with high-order multiple scattering, *Phys. Rev. Lett.,* **75,** 4206–4209.

Derode, A., Tourin, A. & Fink, M., 2001. Random multiple scattering of ultrasound. II. Is time reversal a self-averaging process? *Phys. Rev. E,* **64,** 036606, doi:10.1103/PhysRevE.64.036606.

Ferretti, A., Prati, C. & Rocca, F., 2001. Permanent scatterers in SAR interferometry, *IEEE Trans. Geosci. Remote Sens.,* **39,** 8–20.

Fink, M., Montaldo, G. & Tanter, M., 2003. Time-reversal acoustics in biomedical engineering, *Ann. Rev. Biomed. Eng.,* **5,** 465–497.

Fleury, C. & Vasconcelos, I., 2012. Imaging condition for nonlinear scattering-based imaging: estimate of power loss in scattering, *Geophysics,* **77**(1), S1–S18.

Foldy, L.L., 1945. The multiple scattering of waves. I. General theory of isotropic scattering by randomly distributed scatterers, *Phys. Rev.,* **67,** 107–119.

Fomel, S., 2007. Velocity-independent time-domain seismic imaging using local event slopes, *Geophysics,* **72**(3), S139–S147.

Fomel, S., Landa, E. & Taner, M.T., 2006. Post-stack velocity analysis by separation and imaging of seismic diffractions, in *Proceedings of 76th SEG Meeting,* New Orleans, Louisiana, USA, Expanded Abstracts, pp. 2559–2563.

Galetti, E., Halliday, A. & Curtis, A., 2013. A simple and exact acoustic wavefield modelling code for data processing, imaging and interferometry applications, *Geophysics,* **78,** F17–F27.

Groeneboom, J. & Snieder, R., 1995. Attenuation, dispersion, and anisotropy by multiple scattering of transmitted waves through distributions of scatterers, *J. acoust. Soc. Am.,* **98,** 3482–3492.

Grasmueck, M., Moser, T.J. & Pellisier, M.A., 2012. Stop treating diffractions as noise—use them for imaging of fractures and karts, in *Proceedings of Hedberg Research Conference,* Expanded Abstract.

Hagedoorn, J.G., 1954. A process of seismic reflection interpretation, *Geophys. Prospect.,* **2,** 85–127.

Harlan, W.S., Claerbout, J.F. & Rocca, F., 1984. Signal/noise separation and velocity estimation, *Geophysics,* **49,** 1869–1880.

Insana, M.F. & Brown, D.G., 1993. Acoustic scattering theory applied to soft biological tissues, in *Ultrasonic Scattering in Biological Tissues,* pp. 76–124, CRC Press.

Kanasewich, E. & Phadke, S., 1988. Imaging discontinuities on seismic sections, *Geophysics,* **53,** 334–345.

Khaidukov, V., Landa, E. & Moser, T.J., 2004. Diffraction imaging by focusing-defocusing: an outlook on seismic superresolution, *Geophysics,* **69**(6), 1478–1490.

King, S. & Curtis, A., 2012. Suppressing nonphysical reflections in Green's function estimates using source-receiver interferometry, *Geophysics,* **77**(1), Q15–Q25.

Klem-Musatov, K., 1994. *Theory of Seismic Diffractions,* eds Hron, F. & Lines, L., SEG.

Krey, T., 1952. The significance of diffraction in the investigation of faults, *Geophysics,* **17,** 843–858.

Landa, E. & Keydar, S., 1998. Seismic monitoring of diffraction images for detection of local heterogeneities, *Geophysics,* **63,** 1093–1100.

Landa, E., Shtivelman, V. & Gelchinsky, B., 1987. A method for detection of diffracted waves on common-offset sections, *Geophys. Prospect.,* **35,** 359–374.

Liu, E., Crampin, S. & Hudson, J., 1997. Diffraction of seismic waves by cracks with application to Hydraulic fracturing, *Geophysics,* **62,** 253–265.

Löer, K., Meles, G.A., Curtis, A. & Vasconcelos, I., 2013. Diffracted and pseudo-physical waves from spatially limited arrays using source–receiver interferometry (SRI), *Geophys. J. Int.*, **196**(2), 1043–1059.

Meles, G.A. & Curtis, A., 2013a. Physical and non-physical energy in scattered wave source-receiver interferometry, *J. acoust. Soc. Am.,* **133**(6), 3790–3801.

Meles, G.A. & Curtis, A., 2013b. Discriminating physical and non-physical energy in wavefield interferometry, in *Proceedings of 75th European Association of Geoscientists and Engineers Conference,* Extended Abstract.

Moser, T.J. & Howard, C.B., 2008. Diffraction imaging in depth, *Geophys. Prospect.,* **56,** 627–641.

Papziner, U. & Nick, K.P., 1998. Automatic detection of hyperbolas in georadargrams by slant-stack processing and migration, *First Break,* **16,** 219–223.

Prada, C. & Fink, M., 1994. Eigenmodes of the time reversal operator: a solution to selective focusing in multiple-target media, *Wave Motion,* **20,** 151–163.

Ravasi, M. & Curtis, A., 2013. Elastic imaging with exact wavefield extrapolation for application to ocean-bottom 4C seismic data, *Geophysics,* **78**(6), S265–S284.
Sava, P.C., Biondi, B. & Etgen, J., 2005. Wave-equation migration velocity analysis by focusing diffractions and reflections, *Geophysics,* **70**(3), U19–U27.
Sheriff, R.E., 2002. *Encyclopedic Dictionary of Exploration Geophysics,* Society of Exploration Geophysicists.
Shtivelman, V. & Keydar, S., 2004. Imaging shallow subsurface inhomogeneities by 3D multipath diffraction summation, *First Break,* **23,** 39–42.
Snieder, R., van Wijk, K., Haney, M. & Calvert, R., 2008. Cancellation of spurious arrivals in Green's function extraction and the generalized optical theorem, *Phys. Rev. E,* **78,** 036606.
Soellner, W. & Yang, W., 2002. Diffraction response simulation: a 3D velocity inversion tool, in *Proceedings of 72nd Annual International Meeting,* SEG, Expanded Abstracts, pp. 2293–2296.
Stolt, R. & Benson, A., 1986. *Seismic Migration: theory and Practice*, in *Handbook of Geophysical Exploration,* Vol. 5, Geophysical Press.
Taner, M.T., Fomel, S. & Landa, E., 2006. Separation and imaging of seismic diffractions using plane-wave decomposition, in *Proceedings of 76th SEG meeting,* New Orleans, Louisiana, USA, Expanded Abstracts, pp. 2401–2404.
Wapenaar, K., Slob, E. & Snieder, R., 2010. On seismic interferometry, the generalized optical theorem, and the scattering matrix of a point scatterer, *Geophysics,* **75**(3), SA27–SA35.
Yilmaz, Öz., 2001. *Seismic Data Analysis,* Society of Exploration Geophysics.

APPENDIX: Moveout invariance of diffracted waves

The scattered field due to an arbitrary slowness perturbation distribution $\delta_s(x)$ is described by the non-linear Lippman–Schwinger equation (Stolt & Benson 1986), which in the time domain reads:

$$G^S(x_r, x_s, t) = \int_V 2G_0(x_r, x, t) * \ddot{G}(x, x_s, t)s(x)\delta s(x)\mathrm{d}V, \qquad \text{(A1)}$$

where $*$ indicates convolution, $\ddot{G}$ is the second derivative in time of the Green's function G and $s(x)$ is the slowness.

When the perturbation is due to a set P of point diffractors, the above integral formula reduces to a sum:

$$G^S(x_r, x_s, t) = \sum\nolimits_{d\in P} 2G_0(x_r, x_d, t) * \ddot{G}(x_d, x_s, t)s(x_d)\delta s(x_d). \qquad \text{(A2)}$$

Here, $G(x_d, x_s, t)$ accounts for all of the multiple-diffracted waves that occur between the source at x_s and the scatterer at x_d, while $G_0(x_r, x_d, t)$ describes the waveform connecting the diffractor x_d to the receiver x_r directly, with no scattering. In this formula, x_d is then a 'last' diffractor. Note that no assumptions are made about the model associated with $G_0(x_r, x_d, t)$, which may be arbitrarily inhomogeneous. The scattered field associated with a specific, single last diffractor D is therefore:

$$G^S_D(x_r, x_s, t) \propto G_0(x_r, x_D, t) * \ddot{G}(x_D, x_s, t)s(x_D)\delta s(x_D). \qquad \text{(A3)}$$

The above formula is not suitable for an immediate definition of moveout, as it incorporates more than one arrival (as indicated by red arrows in Fig. A1, which shows waves scattered last at an identical diffractor). Moveout is associated with a single wave front arrival, and therefore requires first the selection of a particular arrival within a gather, and picking of the corresponding arrival time.

When diffracted arrivals are clearly separable (e.g. when the background model is homogenous and only a finite number of scatterers is present), we can order them and define the Nth diffracted waves

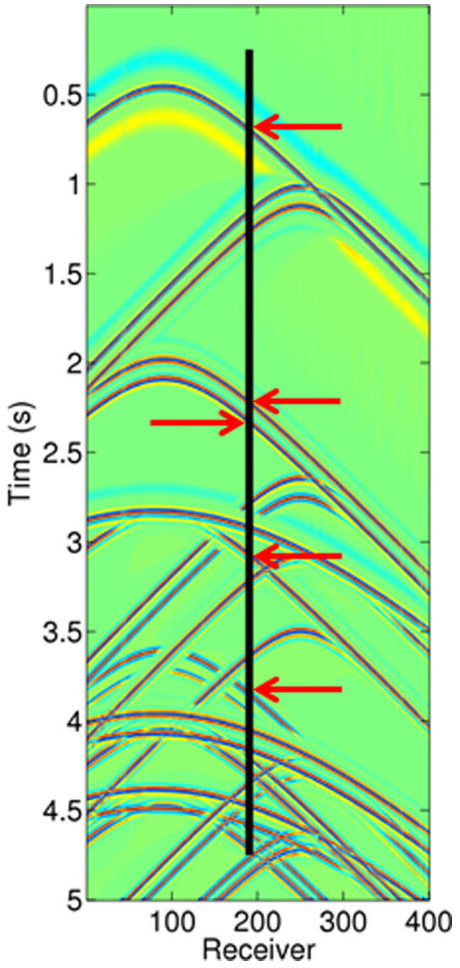

Figure A1. First and higher order waves diffracted last at an identical diffractor exhibit identical moveout in common-source gathers (as indicated by red arrows in A1).

associated with a specific last diffractor as follows:

$$G^S_{D,N}(x_r, x_S, t) \propto G_0(x_r, x_D, t) * {}_N\ddot{G}(x_D, x_S, t)S(x_D)\delta S(x_D), \qquad \text{(A4)}$$

where ${}_N\ddot{G}$ stands for the Nth arrival in the waveform $\ddot{G}$.

We further simplify the problem by introducing a different purely 'spatial' function for any arrival—the traveltime of the analysed scattered wave:

$$T[G^S_{D,N}(x_r, x_s)] \propto T[G_0(x_r, x_D)] + T_N. \qquad \text{(A5)}$$

Here, $T[G^S_{D,N}(x_r, x_s)]$, $T[G_0(x_r, x_D)]$ and T_N indicate the traveltime of $G^S_{D,N}(x_r, x_s)$, $G_0(x_r, x_D, t)$ and ${}_N\ddot{G}(x_D, x_S, t)$, respectively. Whereas waveforms are convolved in (A4), traveltimes are summed in (A5). Because T_N is not a function of x_r, we conclude that the derivative with respect to the receiver position of the waveform, that is, the moveout, only depends on $T[G_0(x_r, x_D)]$:

$$\partial_{x_r} T[G^S_{D,N}(x_r, x_s, t)] \propto \partial_{x_r} T[G_0(x_r, x_D)]. \qquad \text{(A6)}$$

This shows that moving the source x_s can only affect the constant component of the diffracted arrival times observed at an array of receivers (i.e. T_N) but not their variation or moveout across the receiver array. A similar argument for first diffractors and source arrays can easily be derived by invoking source–receiver reciprocity and following a similar procedure.